Journal of
Applied
Crystallography
ISSN 0021-8898

Received 20 June 2011
Accepted 25 January 2012

Polarization-analyzed small-angle neutron scattering. I. Polarized data reduction using *Pol-Corr*

Kathryn Krycka,[a]* Wangchun Chen,[a,b] Julie Borchers,[a] Brian Maranville[a] and Shannon Watson[a]

[a]NIST Center for Neutron Research, National Institute of Standards and Technology, Gaithersburg, Maryland, USA, and [b]Department of Materials Science and Engineering, University of Maryland, College Park, Maryland, USA. Correspondence e-mail: kathryn.krycka@nist.gov

Pol-Corr is a free computer program that corrects for the neutron polarization inefficiencies that are characteristic of polarization-analyzed small-angle neutron scattering experiments, namely those inefficiencies associated with a static neutron polarizer, a neutron spin flipper, beam depolarization and a time-varying neutron spin analyzer. The software is designed to interface directly with small-angle neutron scattering data acquired at the NIST Center for Neutron Research, but the algorithms are generally applicable and can be readily adapted for other data formats. The explicit neutron measurements required to characterize each polarizing element are derived, and these become the input parameters for *Pol-Corr*.

1. Introduction

Polarization-analyzed small-angle neutron scattering (PASANS) is a powerful tool for the unambiguous separation of structural and directionally resolved magnetic scattering (Moon *et al.*, 1969; Schärpf & Capellmann, 1993; Wiedenmann, 2005; Michels & Weissmüller, 2008; Krycka *et al.*, 2009; Honecker *et al.*, 2010), as well as for the separation of coherent and incoherent scattering that is highly pertinent for many biological systems (Gentile *et al.*, 2000; Gaspar *et al.*, 2010). This technique is also referred to as POLARIS (Wiedenmann, 2005; Keiderling *et al.*, 2008) or *XYZ* polarization analysis (Schärpf & Capellmann, 1993; Schweika, 2010). However, the implementation of this technique has been limited because it demands both a neutron spin polarizer for the incident neutron beam and the more rigorous requirement of a spin analyzer capable of capturing a divergent two-dimensional scattered beam, such as a polarized ^{3}He spin filter (Keiderling *et al.*, 2008; Petoukhov *et al.*, 2006; Chen *et al.*, 2009). Additionally, the efficiency of each of these polarizing elements, including the time-dependent ^{3}He spin filter, must be accounted for (Majkrzak, 1991; Keiderling, 2002; Wildes, 2006) in order to reduce and interpret the resulting data properly (described by Krycka *et al.*, 2012). Here, we focus on deriving the experimental neutron-based measurements required to characterize each polarizing element and describe 'user-friendly' software that renders the polarization corrections easy and straightforward. The software presented here, *Pol-Corr*, has been implemented for use with the *Igor Pro*-based SANS reduction suite (Kline, 2006) employed at NIST Center for Neutron Research (NCNR) SANS beamlines, but the approach is general and could be readily adapted to other data formats.

2. Mechanics of PASANS

A typical PASANS setup is shown in Fig. 1, with the incoming beam along the Z axis, the polarization axis along X (as shown) or Z, and a position-sensitive gas detector set in the XY plane. Application of a magnetic guide field (which in practical terms may be as small as several Gauss) defines $\hat{\mathbf{p}}$, about which the neutrons precess at the Larmor frequency. For an unpolarized neutron beam, half the neutron spins will have a projection parallel to $\hat{\mathbf{p}}$ ($\uparrow$) and half antiparallel to $\hat{\mathbf{p}}$ ($\downarrow$). The incident beam is then polarized with a supermirror (*e.g.* an FeSi multilayer diffraction grating) that preferentially selects only one of these spin states ($\uparrow$). However, the subsequent neutron spin orientation may be reversed at will using an electromagnetic precession coil flipper (producing $\downarrow$ neutrons when on and $\uparrow$ neutrons when off). Scattering of the neutron beam from the sample of interest is referred to as

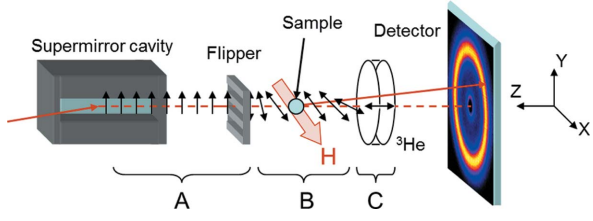

Figure 1
The PASANS setup includes a polarizing supermirror (*e.g.* an FeSi multilayer), an electromagnetic precession coil flipper, a sample holder with cryostat and variable magnetic field, a ^{3}He analyzer, and a position-sensitive gas detector. Arrows indicate the neutron polarization direction, which follows the applied magnetic field, rotating from vertical to horizontal to along the incident-beam direction between the flipper, sample and ^{3}He analyzer, respectively. The system is logically divided into three regions (*A*, *B* and *C*) for the purposes of polarization correction.

spin-flip scattering for $\uparrow \Rightarrow \downarrow$ and $\downarrow \Rightarrow \uparrow$ processes, and non-spin-flip scattering for $\uparrow \Rightarrow \uparrow$ and $\downarrow \Rightarrow \downarrow$ processes. (Comparison of these scattering types allows nuclear and magnetic scattering information to separated.) After interaction with the sample, the neutrons pass through a polarized ^{3}He filter (Keiderling *et al.*, 2008; Petoukhov *et al.*, 2006; Chen *et al.*, 2009), commonly referred to as a ^{3}He analyzing cell. This element works by preferentially allowing neutrons with spin in the same direction as the ^{3}He atoms to pass through, but it is highly absorbing of those neutrons with spin antiparallel to the ^{3}He atoms [*i.e.* ^{3}He($\uparrow$) + neutron($\downarrow$) or ^{3}He($\downarrow$) + neutron($\uparrow$) $\Rightarrow$ ^{4}He(no spin)]. Finally, the orientation of the polarized ^{3}He atoms may be reversed (180° rotation) using a tuned NMR pulse (Jones *et al.*, 2006), with negligible loss of polarization.

Here and in all that follows, superscripted arrows refer to neutrons of that spin orientation, while arrows in subscripted parentheses indicate the majority spin state as set by the polarizing elements. Following this convention, $S_{(\uparrow\uparrow)}$, $S_{(\downarrow\uparrow)}$, $S_{(\downarrow\downarrow)}$ and $S_{(\uparrow\downarrow)}$ refer to experimentally measured scattering patterns, while the corresponding absolute cross sections are given by $\sigma^{\uparrow\uparrow}$, $\sigma^{\downarrow\uparrow}$, $\sigma^{\downarrow\downarrow}$ and $\sigma^{\uparrow\downarrow}$. These cross sections are determined directly from the measured values of S once the polarization efficiency of each element has been characterized and accounted for explicitly (the subject of this article).

With $\uparrow$ as the majority spin state after passage through a polarizing element, such as the supermirror, the polarization, $P_{(\uparrow)}$, is defined as

$$P_{(\uparrow)} \equiv \frac{S^{\uparrow}_{(\uparrow)} - S^{\downarrow}_{(\uparrow)}}{S^{\uparrow}_{(\uparrow)} + S^{\downarrow}_{(\uparrow)}}, \tag{1}$$

and the efficiencies for $\uparrow$ and $\downarrow$ neutrons, $\varepsilon^{\uparrow}_{(\uparrow)}$ and $\varepsilon^{\downarrow}_{(\uparrow)}$, respectively, can be written in terms of $P_{(\uparrow)}$ as

$$\varepsilon^{\uparrow}_{(\uparrow)} \equiv \frac{S^{\uparrow}_{(\uparrow)}}{S^{\uparrow}_{(\uparrow)} + S^{\downarrow}_{(\uparrow)}} = \frac{1 + P_{(\uparrow)}}{2}, \quad \varepsilon^{\downarrow}_{(\uparrow)} \equiv \frac{S^{\downarrow}_{(\uparrow)}}{S^{\uparrow}_{(\uparrow)} + S^{\downarrow}_{(\uparrow)}} = \frac{1 - P_{(\uparrow)}}{2}. \tag{2}$$

Note that for dynamic elements whose intrinsic (atomic) polarization axis may be reversed, such as a ^{3}He analyzer, $P_{(\uparrow)} = P_{(\downarrow)}$. However, for fixed-orientation elements, such as the supermirror and flipper, $P_{(\uparrow)} = -P_{(\downarrow)}$. Thus, we shall define the polarization of the supermirror, $P_{\rm SM} = P_{\rm SM(\uparrow)}$, the polarization of the flipper, $P_{\rm F} = P_{\rm F(\downarrow)}$ with the flipper powered on, and the polarization of the ^{3}He analyzing cell, $P_{\rm cell} = P_{^3{\rm He\ cell(\uparrow)}} = P_{^3{\rm He\ cell(\downarrow)}}$.

Let us consider the polarized beamline setup (Fig. 1) as the sum of three parts: a front-end region, A, comprising a supermirror and a flipper with an associated efficiency ε_A; a middle region, B, containing the sample; and a back-end region, C, occupied by the ^{3}He analyzer with an associated efficiency ε_C. The goal is to extract the absolute sample scattering cross sections, σ_B, from the experimentally measured intensities S by inverting the following matrix (Majkrzak, 1991; Keiderling, 2002; Wildes, 2006):

$$\underbrace{\begin{bmatrix} \varepsilon^{\uparrow}_{A(\uparrow)}\varepsilon^{\uparrow}_{C(\uparrow)} & \varepsilon^{\downarrow}_{A(\uparrow)}\varepsilon^{\uparrow}_{C(\uparrow)} & \varepsilon^{\downarrow}_{A(\uparrow)}\varepsilon^{\downarrow}_{C(\uparrow)} & \varepsilon^{\uparrow}_{A(\uparrow)}\varepsilon^{\downarrow}_{C(\uparrow)} \\ \varepsilon^{\uparrow}_{A(\downarrow)}\varepsilon^{\uparrow}_{C(\uparrow)} & \varepsilon^{\downarrow}_{A(\downarrow)}\varepsilon^{\uparrow}_{C(\uparrow)} & \varepsilon^{\downarrow}_{A(\downarrow)}\varepsilon^{\downarrow}_{C(\uparrow)} & \varepsilon^{\uparrow}_{A(\downarrow)}\varepsilon^{\downarrow}_{C(\uparrow)} \\ \varepsilon^{\uparrow}_{A(\downarrow)}\varepsilon^{\uparrow}_{C(\downarrow)} & \varepsilon^{\downarrow}_{A(\downarrow)}\varepsilon^{\uparrow}_{C(\downarrow)} & \varepsilon^{\downarrow}_{A(\downarrow)}\varepsilon^{\downarrow}_{C(\downarrow)} & \varepsilon^{\uparrow}_{A(\downarrow)}\varepsilon^{\downarrow}_{C(\downarrow)} \\ \varepsilon^{\uparrow}_{A(\uparrow)}\varepsilon^{\uparrow}_{C(\downarrow)} & \varepsilon^{\downarrow}_{A(\uparrow)}\varepsilon^{\uparrow}_{C(\downarrow)} & \varepsilon^{\downarrow}_{A(\uparrow)}\varepsilon^{\downarrow}_{C(\downarrow)} & \varepsilon^{\uparrow}_{A(\uparrow)}\varepsilon^{\downarrow}_{C(\downarrow)} \end{bmatrix}}_{\text{Measured polarization efficiencies}} \underbrace{\begin{bmatrix} \sigma_B^{\uparrow\uparrow} \\ \sigma_B^{\downarrow\uparrow} \\ \sigma_B^{\downarrow\downarrow} \\ \sigma_B^{\uparrow\downarrow} \end{bmatrix}}_{\text{Cross sections}}$$

$$= \underbrace{\begin{bmatrix} S_{(\uparrow\uparrow)} \\ S_{(\downarrow\uparrow)} \\ S_{(\downarrow\downarrow)} \\ S_{(\uparrow\downarrow)} \end{bmatrix}}_{\text{Experimental data}}. \tag{3}$$

Thus, the efficiencies ε_A and ε_C are related to the supermirror, flipper and ^{3}He cell polarizations ($P_{\rm SM}$, $P_{\rm F}$ and $P_{\rm cell}$, respectively) and the unpolarized incident neutron beam transmissions ($T^{\rm unpol\ beam}_{\rm SM}$, $T^{\rm unpol\ beam}_{\rm F} \equiv 1.0$ and $T^{\rm unpol\ beam}_{\rm cell}$, respectively) as follows. With the flipper off ($\uparrow$),

$$\varepsilon^{\uparrow}_{A(\uparrow)} = \left(\frac{1 + P_{\rm SM}}{2}\right) T^{\rm unpol\ beam}_{\rm SM}, \quad \varepsilon^{\downarrow}_{A(\uparrow)} = \left(\frac{1 - P_{\rm SM}}{2}\right) T^{\rm unpol\ beam}_{\rm SM}. \tag{4a}$$

With the flipper on ($\downarrow$),

$$\begin{aligned} \varepsilon^{\downarrow}_{A(\downarrow)} &= \left(\frac{1 + P_{\rm SM}P_{\rm F}}{2}\right) T^{\rm unpol\ beam}_{\rm SM}, \\ \varepsilon^{\uparrow}_{A(\downarrow)} &= \left(\frac{1 - P_{\rm SM}P_{\rm F}}{2}\right) T^{\rm unpol\ beam}_{\rm SM}. \end{aligned} \tag{4b}$$

With the ^{3}He orientation normal ($\uparrow$),

$$\varepsilon^{\uparrow}_{C(\uparrow)} = \left(\frac{1 + P_{\rm cell}}{2}\right) T^{\rm unpol\ beam}_{\rm cell}, \quad \varepsilon^{\downarrow}_{C(\uparrow)} = \left(\frac{1 - P_{\rm cell}}{2}\right) T^{\rm unpol\ beam}_{\rm cell}. \tag{4c}$$

With the ^{3}He orientation reversed ($\downarrow$),

$$\varepsilon^{\downarrow}_{C(\downarrow)} = \left(\frac{1 + P_{\rm cell}}{2}\right) T^{\rm unpol\ beam}_{\rm cell}, \quad \varepsilon^{\uparrow}_{C(\downarrow)} = \left(\frac{1 - P_{\rm cell}}{2}\right) T^{\rm unpol\ beam}_{\rm cell}. \tag{4d}$$

If the scattering data are scaled (§7) by an open-beam (that is, without the sample or analyzer in place) transmission, polarized only by the supermirror, rather than with an unpolarized open-beam transmission, then $T^{\rm unpol\ beam}_{\rm SM}$ is effectively normalized and disappears from equations (4). Additionally, $T^{\rm unpol\ beam}_{\rm cell}$ and $P_{\rm cell}$ may instead be written in terms of the transmission of neutron spins in the majority state (*i.e.* the neutron spin that is parallel to the net ^{3}He direction) and the minority state (the neutron spin that is antiparallel to the net ^{3}He direction) – $T^{\rm majority,\ minority}_{^3{\rm He}}$, discussed further in §4 – as

$$\begin{aligned} \varepsilon^{\uparrow}_{A(\uparrow)} &= \frac{1 + P_{\rm SM}}{2}, \quad \varepsilon^{\downarrow}_{A(\uparrow)} = \frac{1 - P_{\rm SM}}{2}, \\ \varepsilon^{\downarrow}_{A(\downarrow)} &= \frac{1 + P_{\rm SM}P_{\rm F}}{2}, \quad \varepsilon^{\uparrow}_{A(\downarrow)} = \frac{1 - P_{\rm SM}P_{\rm F}}{2}, \\ \varepsilon^{\uparrow}_{C(\uparrow)} &= \varepsilon^{\downarrow}_{C(\downarrow)} = T^{\rm majority}_{^3{\rm He}}, \quad \varepsilon^{\downarrow}_{C(\uparrow)} = \varepsilon^{\uparrow}_{C(\downarrow)} = T^{\rm minority}_{^3{\rm He}}. \end{aligned} \tag{5}$$

From here on, σ_B will simply be referred to as σ, since it should be apparent that the scattering cross section is directly tied to the sample region B.

3. Sample depolarization

Thus far, it has been tacitly assumed that only magnetic scattering originating from the sample itself contributes to flipping of the neutron spin *via* $\sigma^{\uparrow\downarrow}$ and $\sigma^{\downarrow\uparrow}$. However, the orientation of the neutron spins may be flipped whenever they encounter a change in magnetic field direction that is abrupt in comparison with their Larmor precession frequency. Thus, if the orientation of the magnetic guide field fluctuates rapidly, or if the sample contains alternating magnetic domains which the neutron beam passes through, then spin-flip scattering may occur that is not associated with scattering from magnetic moments in the sample. This process is known as depolarization and must be accounted for. Fortunately, as will be demonstrated, depolarization couples directly into the measure of the apparent supermirror polarization.

Let us denote the fraction of neutrons that inadvertently cause spin-flipping independent of sample scattering between the polarizing supermirror and the analyzing ^{3}He cell as χ_D, so that

$$\begin{aligned}
\varepsilon^{\uparrow}_{A(\uparrow)} &= \left(\frac{1+P_{SM}}{2}\right)(1-\chi_D)+\left(\frac{1-P_{SM}}{2}\right)\chi_D,\\
\varepsilon^{\downarrow}_{A(\uparrow)} &= \left(\frac{1-P_{SM}}{2}\right)(1-\chi_D)+\left(\frac{1+P_{SM}}{2}\right)\chi_D,\\
\varepsilon^{\downarrow}_{A(\downarrow)} &= \left(\frac{1+P_{SM}P_F}{2}\right)(1-\chi_D)+\left(\frac{1-P_{SM}P_F}{2}\right)\chi_D,\\
\varepsilon^{\uparrow}_{A(\downarrow)} &= \left(\frac{1-P_{SM}P_F}{2}\right)(1-\chi_D)+\left(\frac{1+P_{SM}P_F}{2}\right)\chi_D.
\end{aligned} \tag{6}$$

Note that if the supermirror polarization multiplied by the sample depolarization term, $P_{SM}(1-2\chi_D)$, is replaced by P'_{SM} then equations (6) reduce to the form of equations (5), demonstrating the coupling of P_{SM} and χ_D. In practical terms, this means that if a sample condition is varied in a manner that might potentially alter χ_D, then a new P'_{SM} should always be measured.

4. ^{3}He efficiency

In characterizing the performance of the polarizing elements it is assumed that the measured transmissions are consistently normalized by either the counting time or the monitor counts. The basic ^{3}He equation governing the transmission of the neutron spins in the majority state (*i.e.* the neutron spin that is parallel to ^{3}He) and the minority state (neutron spin that is antiparallel to ^{3}He) (Chen *et al.*, 2009) is

$$T_{^3\mathrm{He}}^{\text{majority, minority}} = T_E \exp\left[-\mu(1 \mp \wp_{^3\mathrm{He}})\right], \tag{7}$$

where T_E is the transmission of an unfilled cell (known *a priori*), μ is the neutron attenuation length or opacity, and $\wp_{^3\mathrm{He}}$ is the polarization of the ^{3}He atoms, which is not equivalent to the polarization of the ^{3}He cell (P_{cell}) as observed by neutrons. Note that, for an unpolarized neutron beam, the number of incident, parallel and antiparallel neutrons encountering the ^{3}He cell should be equal, and we can write $T_{^3\mathrm{He}}^{\text{unpol beam}} = T_{^3\mathrm{He}}^{\text{majority}} + T_{^3\mathrm{He}}^{\text{minority}}$. When the ^{3}He cell is depolarized, $\wp_{^3\mathrm{He}} \Rightarrow 0$, and μ can be measured using the following equation,

$$\begin{aligned}
\mu &= -\ln\left(\frac{T_{^3\mathrm{He}}^{\text{majority}} + T_{^3\mathrm{He}}^{\text{minority}}}{T_E}\right)\\
&= -\ln\left[\left(\frac{1}{T_E}\right)\frac{T_{\text{unpolarized }^3\text{He cell}}^{\text{unpol beam}} - T_{\text{background noise}}}{T_{^3\text{He cell OUT}}^{\text{unpol beam}} - T_{\text{background noise}}}\right],
\end{aligned} \tag{8}$$

where $T_{\text{background noise}}$ refers to the electronic dark noise plus the detector counts originating from nearby neutron sources, both of which can be measured with a sufficiently thick beam block placed close to the sample position. The superscript 'unpol beam' means that the supermirror polarizer has been removed from the neutron beam path, while the subscript '^{3}He cell OUT' indicates that the ^{3}He cell has been translated away from the neutron beam. Since μ is expected to remain constant as a function of time, this optional measurement is used either as a consistency check or to increase the measurement statistics of μ. Such measurements involve a ^{3}He cell in a fully depolarized state and the repolarization of the ^{3}He takes time. Thus, this procedure is usually performed at the end of an experiment, if at all.

Conversely, if an unpolarized beam is applied to a polarized ^{3}He cell (the usual state of ^{3}He in a PASANS experiment) then we can write the transmission in terms of $\wp_{^3\mathrm{He}}$ as

$$\begin{aligned}
T_{^3\mathrm{He}}^{\text{unpol beam}} &= \left(T_{^3\mathrm{He}}^{\text{majority}} + T_{^3\mathrm{He}}^{\text{minority}}\right)/2\\
&= \frac{T_E}{2}\left\{\exp\left[-\mu(1-\wp_{^3\mathrm{He}})\right] + \exp\left[-\mu(1+\wp_{^3\mathrm{He}})\right]\right\}\\
&= T_E \exp(-\mu)\cosh(\mu\wp_{^3\mathrm{He}}).
\end{aligned} \tag{9}$$

Experimentally, this means that the polarization of the ^{3}He atoms can be measured using

$$\wp_{^3\mathrm{He}} = a\cosh\left[\frac{T_{(\text{polarized})^3\text{He cell}}^{\text{unpol beam}} - T_{\text{background noise}}}{T_{^3\text{He cell OUT}}^{\text{unpol beam}} - T_{\text{background noise}}}\frac{1}{T_E\exp(-\mu)}\right]/\mu. \tag{10}$$

Finally, the effective polarization of the ^{3}He cell from the neutron perspective, P_{cell}, depends on $\wp_{^3\mathrm{He}}$ as

$$\begin{aligned}
P_{cell} &\equiv \left|\frac{T_{^3\mathrm{He}}^{\text{majority}} - T_{^3\mathrm{He}}^{\text{minority}}}{T_{^3\mathrm{He}}^{\text{majority}} + T_{^3\mathrm{He}}^{\text{minority}}}\right| = \frac{T_E\exp(-\mu)\sinh(\mu\wp_{^3\mathrm{He}})}{T_E\exp(-\mu)\cosh(\mu\wp_{^3\mathrm{He}})}\\
&= \tanh(\mu\wp_{^3\mathrm{He}}).
\end{aligned} \tag{11}$$

5. ^{3}He time dependence

The polarization of the ^{3}He cell typically has an associated time dependence to be considered. ^{3}He atoms are optically pumped into a polarized state using circularly polarized laser light (Chen *et al.*, 2009). This procedure is often performed at a location away from the beamline over the course of several

days. Once the optically pumping light source is removed, the ^{3}He slowly loses polarization, with a time constant, Γ, of the order of tens to hundreds of hours, depending on the magnetic field conditions to which the ^{3}He is exposed. Thus, the ^{3}He time dependence can be described using

$$\mu\wp_{^3\mathrm{He}}(t_n) = \mu\wp_{^3\mathrm{He}}(t_0)\exp\left[(t_0 - t_n)/\Gamma\right], \tag{12}$$

where t_0 is the start time at which the first polarization measurement was obtained and t_n is any subsequent time of interest. Although it would be possible to measure P_{cell} experimentally before or after each scattering file for the purposes of polarization correction, we feel it is superior to measure P_{cell} [equation (11)] at a series of times over the entire period of usage for a given ^{3}He cell. Fitting these discrete measurements of $\wp_{^3\mathrm{He}(t_n)}$ *versus* time (t_n) yields a global Γ and $\wp_{^3\mathrm{He}}(t_0)$, from which $\wp_{^3\mathrm{He}(t_n)}$ and $P_{\mathrm{cell}}(t_n)$ can be calculated at any time using equation (12). Fig. 2 demonstrates one such spreadsheet calculation available to users (software is available at http://www.ncnr.nist.gov/equipment/he3nsf/index.html). For practical purposes, data collection of up to an hour or two per scan for ^{3}He cells with Γ of 100 h or more can be corrected quite well using a single time-averaged value of $P_{\mathrm{cell}}(t_n)$. Note that if the experiment happens to employ continuous *in situ* pumping, such that the ^{3}He polarization remains static throughout the experiment, then a single measurement of $\wp_{^3\mathrm{He}}(t_0)$ is required and Γ can effectively be thought of as tending towards infinity for use with the *Pol-Corr* software. The beauty of incorporating an independent decay parameter directly into the polarization correction procedure, even for an *in situ* setup, is that any change of polarization, ranging from a slight polarization loss in cell flipping to a slow degradation from stray magnetic fields that *in situ* pumping may not be able compensate for, can be accounted for with relative ease.

6. Flipper and supermirror efficiencies

Polarized beam transmissions are denoted by $T_{(\uparrow\uparrow)}$, $T_{(\downarrow\uparrow)}$, $T_{(\downarrow\downarrow)}$ and $T_{(\uparrow\downarrow)}$, and they replace the respective scattering measurements $S_{(\uparrow\uparrow)}$, $S_{(\downarrow\uparrow)}$, $S_{(\downarrow\downarrow)}$ and $S_{(\uparrow\downarrow)}$ in equation (3). Changing from scattering to transmission necessitates that the scattering cross sections, σ, be replaced by the fraction of non-absorbed and non-scattered neutrons that pass through the sample area (region B in Fig. 1), denoted $\mathcal{F}^{\uparrow\uparrow}$, $\mathcal{F}^{\downarrow\uparrow}$, $\mathcal{F}^{\downarrow\downarrow}$ and $\mathcal{F}^{\downarrow\uparrow}$. The advantage of using transmission measurements in place of scattering measurements is that, since the contributing scattering processes are negligibly small, $\mathcal{F}^{\downarrow\uparrow} = \mathcal{F}^{\uparrow\downarrow} = 0$, while $\mathcal{F}^{\uparrow\uparrow} = \mathcal{F}^{\downarrow\downarrow} \equiv \kappa$, where κ is a constant. Thus, equations (3) and (5) reduce to

$$\begin{aligned}
T_{(\uparrow\uparrow)} &= \kappa\left[\left(\frac{1+P'_{\mathrm{SM}}}{2}\right)\left(\frac{1+P_{\mathrm{cell}}}{2}\right) + \left(\frac{1-P'_{\mathrm{SM}}}{2}\right)\left(\frac{1-P_{\mathrm{cell}}}{2}\right)\right]T_{^3\mathrm{He}}^{\mathrm{unpol\,beam}},\\
T_{(\uparrow\downarrow)} &= \kappa\left[\left(\frac{1+P'_{\mathrm{SM}}}{2}\right)\left(\frac{1-P_{\mathrm{cell}}}{2}\right) + \left(\frac{1-P'_{\mathrm{SM}}}{2}\right)\left(\frac{1+P_{\mathrm{cell}}}{2}\right)\right]T_{^3\mathrm{He}}^{\mathrm{unpol\,beam}},\\
T_{(\downarrow\downarrow)} &= \kappa\left[\left(\frac{1+P'_{\mathrm{SM}}P_{\mathrm{F}}}{2}\right)\left(\frac{1+P_{\mathrm{cell}}}{2}\right) + \left(\frac{1-P'_{\mathrm{SM}}P_{\mathrm{F}}}{2}\right)\left(\frac{1-P_{\mathrm{cell}}}{2}\right)\right]T_{^3\mathrm{He}}^{\mathrm{unpol\,beam}},\\
T_{(\downarrow\uparrow)} &= \kappa\left[\left(\frac{1+P'_{\mathrm{SM}}P_{\mathrm{F}}}{2}\right)\left(\frac{1-P_{\mathrm{cell}}}{2}\right) + \left(\frac{1-P'_{\mathrm{SM}}P_{\mathrm{F}}}{2}\right)\left(\frac{1+P_{\mathrm{cell}}}{2}\right)\right]T_{^3\mathrm{He}}^{\mathrm{unpol\,beam}}.
\end{aligned} \tag{13}$$

From these four transmission measurements, P'_{SM} and $P'_{\mathrm{SM}}P_{\mathrm{F}}$ can be determined, with known $T_{^3\mathrm{He}}^{\mathrm{unpol\,beam}}(t_n)$ and $P_{\mathrm{cell}}(t_n)$ [equations (7) and (11)], using

$$P'_{\mathrm{SM}} = \frac{T_{(\uparrow\uparrow)}(t_1)/T_{^3\mathrm{He}}^{\mathrm{unpol\,beam}}(t_1) - T_{(\uparrow\downarrow)}(t_2)/T_{^3\mathrm{He}}^{\mathrm{unpol\,beam}}(t_2)}{P_{\mathrm{cell}}(t_1) + P_{\mathrm{cell}}(t_2)} \tag{14}$$

and

Measurement	Time (hrs)	Det. Cnts.	Monitor Rate	Time (sec)	Relative Time	P 3He atoms	P 3He Cell	T Majority Spins	T Minority Spins
T w. 3He	17.8	58086	15555.1	180					
T w/o 3He		398773	15540.8	180					
T blocked		408	15543.7	180	0	0.6474	0.9662	0.2844	0.0049
T w. 3He	21.68	4614	15554.4	180					
T w/o 3He		29672	15540.1	180					
T blocked		958	15526.2	180	3.88	0.6046	0.9560	0.2487	0.0056
T w. 3He	25.65	4021	15522.9	180					
T w/o 3He		30297	15522.9	180					
T blocked		958	15526.2	180	7.85	0.5382	0.9340	0.2019	0.0069
T w. 3He	33.03	3426	15520	180					
T w/o 3He		30426	15555.6	180					
T blocked		958	15526.2	180	15.23	0.4624	0.8959	0.1592	0.0087
T w. 3He	37.48	3147	15540.9	180					
T w/o 3He		30891	15555.2	180					
T blocked		958	15526.2	180	19.68	0.4126	0.8603	0.1361	0.0102
T w. 3He	41.73	26137	15528.6	180					
T w/o 3He		394065	15546.5	180					
T blocked		408	15544.9	180	23.93	0.3703	0.8216	0.1192	0.0117

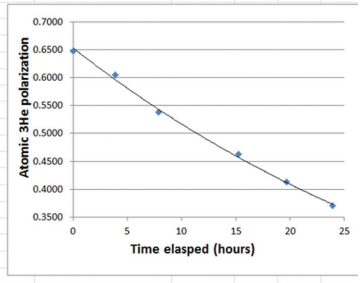

Pol 3He (intercept):	0.653
Gamma (inverse slop	42.7

Figure 2
Calculating ^{3}He polarization time dependence using a spreadsheet. The user enters unpolarized transmission values for ^{3}He in and out of the neutron beam, resulting in fit-determined values for Γ and $\wp_{^3\mathrm{He}}(t_0)$. Although values of Γ in excess of 200 h are routinely achieved at the NCNR, data from a magnetic field-reduced Γ are presented here for the purposes of illustration.

$$P'_{\rm SM}P_{\rm F} = \frac{T_{(\downarrow\downarrow)}(t_1)/T^{\rm unpol\,beam}_{^3{\rm He}}(t_1) - T_{(\downarrow\uparrow)}(t_2)/T^{\rm unpol\,beam}_{^3{\rm He}}(t_2)}{P_{\rm cell}(t_1) + P_{\rm cell}(t_2)}, \tag{15}$$

where $P_{\rm F}$ may obviously be extracted from equations (14) and (15). Separation becomes particularly simple if all four transmissions are taken back-to-back at approximately the same time, t_n,

$$P_{\rm F} = \frac{T_{(\downarrow\downarrow)}(t_n) - T_{(\downarrow\uparrow)}(t_n)}{T_{(\uparrow\uparrow)}(t_n) - T_{(\uparrow\downarrow)}(t_n)} \tag{16}$$

and

$$\begin{aligned} P'_{\rm SM} &= \frac{T_{(\uparrow\uparrow)}(t_n) - T_{(\uparrow\downarrow)}(t_n)}{2P_{\rm cell}(t_n)} = \frac{T_{(\downarrow\downarrow)}(t_n) - T_{(\downarrow\uparrow)}(t_n)}{2P_{\rm F}P_{\rm cell}(t_n)} \\ &= \frac{T_{(\uparrow\uparrow)}(t_n) - T_{(\downarrow\uparrow)}(t_n)}{P_{\rm cell}(t_n)(1+P_{\rm F})} = \frac{T_{(\downarrow\downarrow)}(t_n) - T_{(\uparrow\downarrow)}(t_n)}{P_{\rm cell}(t_n)(1+P_{\rm F})}. \end{aligned} \tag{17}$$

While $P_{\rm F}$ should remain constant over the course of an experiment for a given wavelength, $P'_{\rm SM}$ depends directly on the sample conditions. Thus, $P'_{\rm SM}$ must be remeasured for each new condition of applied magnetic field, temperature, wavelength, sample thickness *etc.* that might potentially alter $\chi_{\rm D}$.

7. Absolute-scale scattering cross sections

In addition to correcting for the polarization leakage from each of the polarizing elements, the two-dimensional scattering data must be scaled by the neutron flux, and corrected for sample absorption and transmission loss through the ^{3}He spin filter, in order to be converted into an absolute-scale cross section. The neutron flux and sample absorption corrections may be performed within the *Igor Pro*-based SANS reduction suite (Kline, 2006), requiring only an open-beam transmission, $T_{\rm sample\,OUT,\,^3He\,OUT}$, a sample transmission, $T_{\rm sample,\,^3He\,OUT}$, and a blocked-beam scattering file, $S_{\rm background\ noise}$. As noted, if these measurements are taken with the supermirror in place, then $T^{\rm unpol\,beam}_{\rm SM}$ may be neglected and equations (5) may be used directly. Using the *Igor Pro*-based SANS reduction procedure has the added advantage of additionally correcting for the geometric effects associated with intersecting a spherical wavefront with a flat detector and for the effect of gravity between the point of scattering and the distance traveled to the detector (Kline, 2006). The re-scaled and geometrically corrected scattering files may be exported into ASCII format, retaining the full pixel-by-pixel spatial delineation, for further correction.

With experimentally determined knowledge of $T_{\rm E}$, μ, Γ, $\wp_{^3{\rm He}}(t_0)$, $P_{\rm F}$ and $P'_{\rm SM}$ (described above), the polarization leakage and ^{3}He absorption may be rectified using equations (3) and (5) (Majkrzak, 1991; Keiderling, 2002; Wildes, 2006). To facilitate this, we introduce the software package *Pol-Corr* (snapshots of its relevant parts are shown Fig. 3). It is written in C (software available at http://www.ncnr.nist.gov/equipment/he3nsf/index.html) and wrapped into a *LabVIEW* graphical user interface for ease of use. Users do not need to have a *LabVIEW* license, but rather can interface with the executable application using the free *LabVIEW* Runtime Engine 9.0 (National Instruments, Austin, Texas, USA). Multiple monitor-normalized scattering files may be summed together within a given spin orientation (*i.e.* $\uparrow\uparrow$, $\downarrow\uparrow$, $\downarrow\downarrow$ or $\uparrow\downarrow$) for increased statistics, with their associated $\varepsilon_A\varepsilon_C$ terms linearly summed together. The number of files recorded for each orientation need not be the same, nor must the scattering files be recorded using the same ^{3}He cell, though the number of files per spin-state orientation is limited to five within *Pol-Corr* (Fig. 3*a*). The time stamp taken from the header file of each scattering file can be used to determine the time elapsed since the $\wp_{^3{\rm He}}(t_0)$ of the appropriate ^{3}He cell was measured, which, in combination with Γ, determines the time-corrected $T^{\rm majority,\,minority}_{^3{\rm He}}$ ($P_{\rm cell}$) for each scattering file. Each scattering file must be correlated with one of a possible three associated ^{3}He cells (Fig. 3*a*), labeled 0–2 (Fig. 3*b*), and associated with an output file name. $P_{\rm F}$ and $P_{\rm SM}$ values are entered manually, allowing the user to explore fully the effects of varying these calculated parameters within uncertainty limits. Once all the appropriate information has been entered, the user triggers the program to perform the polarization correction on the data, and the resulting four corrected cross sections ($\sigma^{\uparrow\uparrow}$, $\sigma^{\downarrow\uparrow}$, $\sigma^{\downarrow\downarrow}$ and $\sigma^{\uparrow\downarrow}$) are displayed as linear or logarithmic images (Fig. 3*c*). The polarization-corrected ASCII output files thus generated may be imported back into the SANS reduction software for further analysis.

Polarized background scattering files (that is, scattering files collected with all apparatus in place except for the sample itself) have their own distinct ^{3}He time dependence, and so they should be polarization corrected before being subtracted. If the background contains no magnetic material, as is typical, it is valid to assume that $\sigma^{\uparrow\uparrow} = \sigma^{\downarrow\downarrow} \equiv \sigma^{\rm NSF}$ and $\sigma^{\downarrow\uparrow} = \sigma^{\uparrow\downarrow} \equiv \sigma^{\rm SF}$. For this case, $S_{(\uparrow\uparrow)}$ and $S_{(\uparrow\downarrow)}$ differ from $S_{(\downarrow\downarrow)}$ and $S_{(\downarrow\uparrow)}$, respectively, only in their dependence on $P_{\rm F}$. Thus, if $P_{\rm F}$ is set to unity, it is possible to measure only $S_{(\uparrow\uparrow)}$ and $S_{(\uparrow\downarrow)}$ in place of $S_{(\uparrow\uparrow)}$, $S_{(\downarrow\downarrow)}$ and $S_{(\uparrow\downarrow)}$, $S_{(\downarrow\uparrow)}$, and to correct them for polarization using the standard *Pol-Corr* reduction framework. This procedure has the advantage of reducing the number of required background scattering files by a factor of two.

Uncertainty within the polarization-correction framework is composed of both random (statistical counting fluctuations) and systematic (uncertainty of the combined polarized element efficiencies) errors. A change in one or more of the polarization efficiencies has the primary affect of globally scaling the cross sections as a function of $\mathbf{Q}$ [$Q = |\mathbf{Q}| = (4\pi/\lambda)\sin(\theta/2)$, where θ is the scattering angle and λ is the wavelength of the incident radiation], rather than altering the scattering profile shape as a function of $\mathbf{Q}$. While it is possible to propagate the combined sources of uncertainty through the matrix inversion process by calculating a covariance matrix (Lefebvre *et al.*, 2000), this is likely to underestimate the data quality and the significance of scattering shape/slope as a function of $\mathbf{Q}$. Thus, we instead propose retaining only the statistical errors [as is customary for SANS, as described by Kline (2006)] per set of polarization parameters, but performing this operation several times, using the average

polarization values, the combination of polarization values that maximize the degree of polarization correction within one standard deviation and the combination of polarization values that minimize the degree of polarization correction within one standard deviation. In such an approach, the statistical errors would dictate how much significance should be given to the

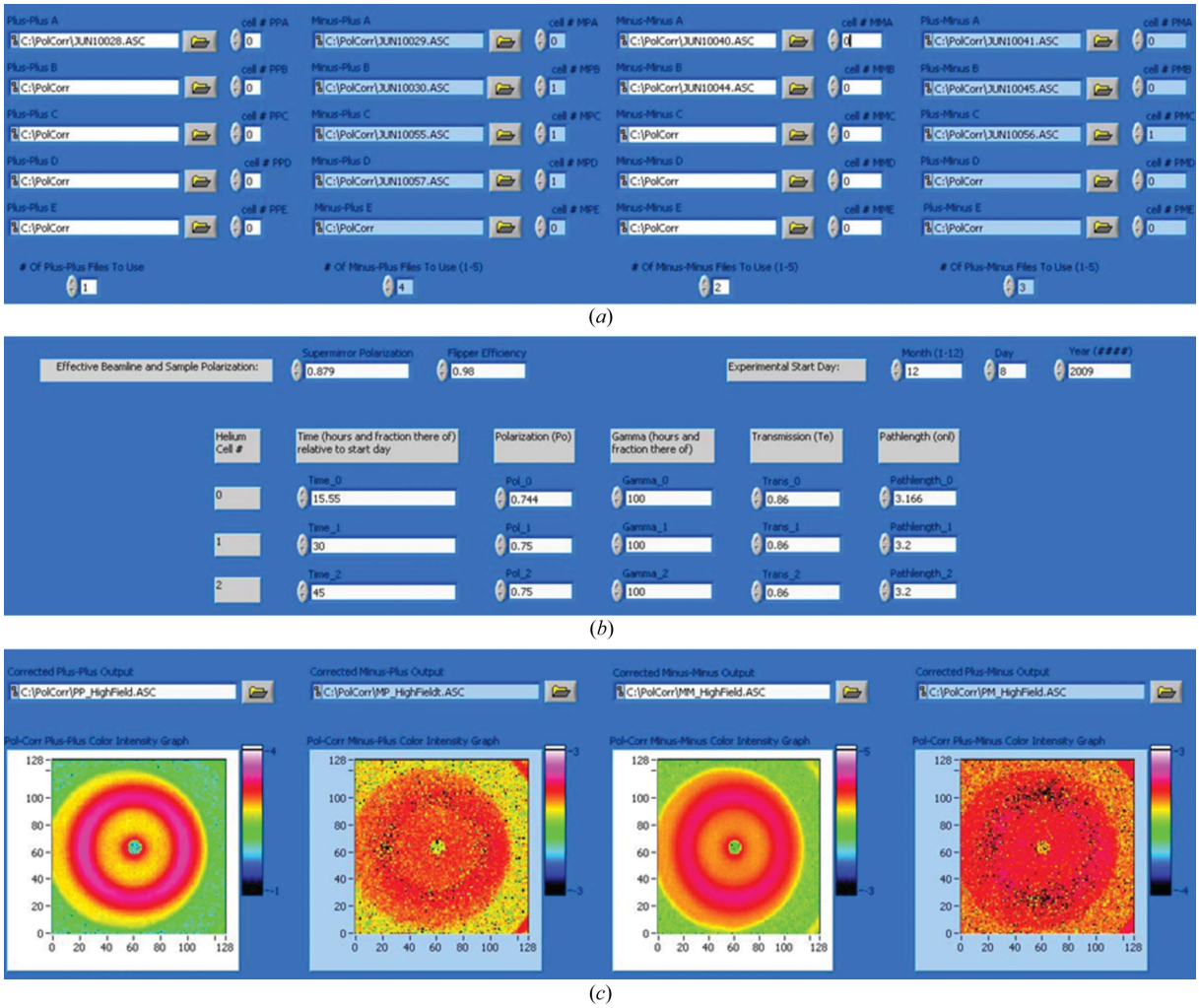

(*a*)

(*b*)

(*c*)

Figure 3
The *Pol-Corr* software allows users (*a*) to enter up to five scattering files apiece for $I_{(\uparrow\uparrow)}$, $I_{(\downarrow\uparrow)}$, $I_{(\downarrow\downarrow)}$ and $I_{(\uparrow\downarrow)}$ and to associate a ^{3}He cell with each file; (*b*) to specify P_F and P'_{SM} and up to three ^{3}He cells, each with their own unique time dependence; and (*c*) to view the resulting two-dimensional polarization-corrected user-named ASCII files.

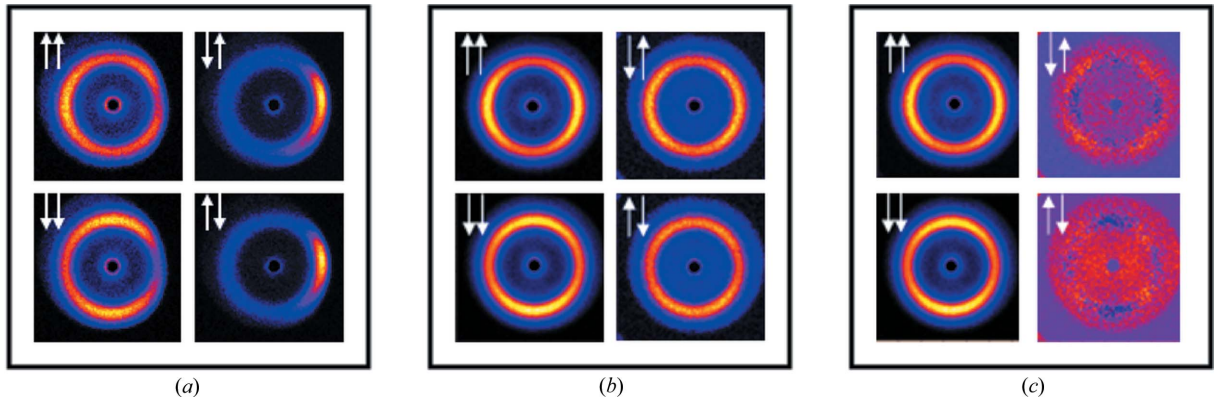

(*a*) (*b*) (*c*)

Figure 4
The effects of correction. (*a*) Structural–magnetic Bragg peak from a sample reported by Krycka *et al.* (2010), with severe depolarization on the right-hand side. (*b*) Scattering after depolarization is removed experimentally with added shielding that limits stray magnetic fields. (*c*) The sample scattering after polarization correction has been applied. Note how the fine features in the spin-flip scattering become apparent.

Table 1
Experimental measurements and their usage.

Unless otherwise noted, the supermirror, sample and polarized ^{3}He cell should be in the neutron beam.

Variable(s) to be solved	Known variable(s)	Experimental measurements	Equations to be used
μ (optional)	$T_{\rm E}$	$T^{\rm unpol\ beam}_{\rm unpolarized\ ^3He\ cell}$, $T^{\rm unpol\ beam}_{^3{\rm He\ cell\ OUT}}$, $T_{\rm background\ noise}$	(8)
$\wp_{^3{\rm He}}(t_n)$	$T_{\rm E}$, μ	$T^{\rm unpol\ beam}_{\rm (polarized)\ ^3He\ cell}$, $T^{\rm unpol\ beam}_{^3{\rm He\ cell\ OUT}}$, $T_{\rm background\ noise}$	(10)
$P_{\rm cell}(t_n)$	$\wp_{^3{\rm He}}(t_n)$	No additional measurements	(11)
$T^{\rm majority,\ minority}_{^3{\rm He\ cell}}(t_n)$	$\wp_{^3{\rm He}}(t_n)$	No additional measurements	(7)
Γ, $\wp_{^3{\rm He}}(t_0)$	Series of $\wp_{^3{\rm He}}(t_n)$	Graph of $\wp_{^3{\rm He}}(t_n)$ *versus* t_n	(12)
$P'_{\rm SM}$	$P_{\rm cell}(t_1)$, $P_{\rm cell}(t_2)$, $T^{\rm unpol\ beam}_{^3{\rm He\ cell}}(t_1)$, $T^{\rm unpol\ beam}_{^3{\rm He\ cell}}(t_2)$	$T_{(\uparrow\uparrow)}(t_1)$, $T_{(\uparrow\downarrow)}(t_2)$	(14)
$P'_{\rm SM}P_{\rm F}$	$P_{\rm cell}(t_1)$, $P_{\rm cell}(t_2)$, $T^{\rm unpol\ beam}_{^3{\rm He\ cell}}(t_1)$, $T^{\rm unpol\ beam}_{^3{\rm He\ cell}}(t_2)$	$T_{(\downarrow\downarrow)}(t_1)$, $T_{(\downarrow\uparrow)}(t_2)$	(15)
$P_{\rm F}$ independent of $P'_{\rm SM}$	None	$T_{(\uparrow\uparrow)}(t_n)$, $T_{(\downarrow\uparrow)}(t_n)$, $T_{(\downarrow\downarrow)}(t_n)$ and $T_{(\uparrow\downarrow)}(t_n)$ taken back to back	(16)
$\sigma^{\uparrow\uparrow}$, $\sigma^{\downarrow\uparrow}$, $\sigma^{\downarrow\downarrow}$, $\sigma^{\uparrow\downarrow}$	$T_{\rm E}$, μ, Γ, $\wp_{^3{\rm He}}(t_n)$, $P_{\rm F}$, $P'_{\rm SM}$	†$S_{(\uparrow\uparrow)}$, $S_{(\downarrow\uparrow)}$, $S_{(\downarrow\downarrow)}$, $S_{(\uparrow\downarrow)}$; ‡$S_{\rm background\ noise}$; $T_{\rm sample\ IN,\ ^3He\ cell\ OUT}$; $T_{\rm sample\ OUT,\ ^3He\ cell\ OUT}$	(3), (5)

† $S_{\rm background\ noise}$, $S_{(\uparrow\uparrow)}$, $S_{(\downarrow\uparrow)}$, $S_{(\downarrow\downarrow)}$, $S_{(\uparrow\downarrow)}$, $T_{\rm sample\ OUT,\ ^3He\ cell\ OUT}$ and $T_{\rm sample\ IN,\ ^3He\ cell\ OUT}$ should be acquired and polarization corrected separately for each condition, including the condition of 'background'. ‡ Blocked-beam measurements of $S_{\rm background\ noise}$ and $T_{\rm background\ noise}$ may differ, owing to differences in attenuation and presence of the beam stop.

scattering shape, while the family of solutions taken together would dictate the uncertainty of the absolute scaling.

8. Effect of depolarization and polarization leakage

Fig. 4 demonstrates the relative effects of polarization leakage correction (going from Figs. 4*b* to 4*c*) and stray magnetic field depolarization (going from Figs. 4*a* to 4*b*), both of which can play an important role in data processing. For all images in Fig. 4, the scattering subject consisted of 9 nm Fe_3O_4 nanoparticles close packed into crystallites, giving rise to the interparticle Bragg peak observed as a bright diffraction ring in Fig. 4 (Krycka *et al.*, 2010). When one considers the facts that non-spin-flip scattering is usually dominated by structural scattering, that the spin-flip scattering is magnetic only in origin and that the ratio of the latter to the former is typically very small (3–4% at most for magnetically saturated Fe_3O_4, for example), then it becomes obvious that polarization correction is often critical for a correct interpretation of magnetic scattering. For example, the values of $P'_{\rm SM}$ and $P_{\rm F}$ calculated for the data shown in Fig. 4 were somewhat low [0.879 (6) and 0.987 (5), respectively], in part because of non-trivial sample depolarization. However, even with perfect supermirror and flipper optics, sample depolarization and the time-dependence of the ^{3}He cell polarization would still have required correction in order to interpret and analyze the data meaningfully.

With regard to the issue of non-uniform or stray-field depolarization, it is imperative that the transmission measurements (taken about $|\mathbf{Q}| = 0$) accurately represent the polarization efficiency for all $\mathbf{Q}$ of interest. Fortunately, sample depolarization affects the scattering neutron beam fairly evenly as a function of $\mathbf{Q}$, and thus it can usually be well accounted for within $P'_{\rm SM}$. However, stray fields arising from nearby superconducting magnets or electromagnets may interact with the neutron beam once it has started to diverge and, therefore, may only affect a specific region of $\mathbf{Q}$ [see right-hand side of scattering images in Fig. 4(*a*), for example]. Thus, upon starting a new experiment, users are strongly encouraged to check for the presence of gross depolarization regions [typically observed as asymmetric bright regions in $S_{(\uparrow\downarrow)}$, $S_{(\downarrow\uparrow)}$ and dark low-intensity regions in $S_{(\uparrow\uparrow)}$, $S_{(\downarrow\downarrow)}$, when nuclear scattering is expected to dominate the magnetic scattering contributions]. If such asymmetries are seen, it is highly advisable to correct for them physically, for example by increasing the distance between high-field magnets and the ^{3}He analyzer when space is available, increasing the neutron magnetic guide fields, or adding additional magnetic (mu-metal) shielding (Fig. 4*b*), since *Pol-Corr* and similar polarization-correction approaches will not be able to correct these regions properly.

9. Duration of ^{3}He cell usage

Determining the optimal time for exchanging the ^{3}He cell for a freshly polarized one – considering that each cell exchange reduces the experimental counting time available, while using a cell for too long can significantly increase polarization inefficiency and reduce neutron transmission – is somewhat complex. One common tactic used to access the state of the ^{3}He quickly is the measurement of a flipping ratio (FR), which is the ratio of the non-spin-flip state to the corresponding spin-flip state measured with only the flipper condition altered (on to off or off to on). Re-writing equation (13), we obtain

$$\begin{aligned}
{\rm FR}_{(\uparrow\uparrow/\downarrow\uparrow)} &\equiv \frac{T_{(\uparrow\uparrow)}(t_n) - T_{\rm background\ noise}}{T_{(\downarrow\uparrow)}(t_n) - T_{\rm background\ noise}} \\
&= \frac{(1+P'_{\rm SM})[1+P_{\rm cell}(t_n)] + (1-P'_{\rm SM})[1-P_{\rm cell}(t_n)]}{(1-P'_{\rm SM}P_{\rm F})[1+P_{\rm cell}(t_n)] + (1+P'_{\rm SM}P_{\rm F})[1-P_{\rm cell}(t_n)]}, \\
{\rm FR}_{(\downarrow\downarrow/\uparrow\downarrow)} &\equiv \frac{T_{(\downarrow\downarrow)}(t_n) - T_{\rm background\ noise}}{T_{(\uparrow\downarrow)}(t_n) - T_{\rm background\ noise}} \\
&= \frac{(1-P'_{\rm SM}P_{\rm F})[1-P_{\rm cell}(t_n)] + (1+P'_{\rm SM}P_{\rm F})[1+P_{\rm cell}(t_n)]}{(1+P'_{\rm SM})[1-P_{\rm cell}(t_n)] + (1-P'_{\rm SM})[1+P_{\rm cell}(t_n)]}.
\end{aligned} \tag{18}$$

Since $\mathcal{F}^{\uparrow\downarrow}$ and $\mathcal{F}^{\downarrow\uparrow}$ are negligible in transmission, the denominators of equations (18) are a good measure of leakage from non-spin-flip transmission into the observed spin-flip transmission. Meanwhile, the numerators very closely approximate the level non-spin-flip transmission one would expect if the system experienced no leakage. Thus, the values of FR^{-1} are a good measure of the level of leakage one might expect to see in a spin-flip scattering channel, normalized by the non-spin-flip scattering. However, the situation is compounded by the fact that, as P_{cell} (and also $\wp_{^3\mathrm{He}}$) decreases, the transmission of the majority spin state through the ^{3}He also substantially decreases [equation (7)]. In Fig. 2, for example, a modest decrease in P_{cell} from 0.97 to 0.82 leads to a majority spin-state transmission of 0.28 to 0.12 – a reduction of more than 2. Thus, it is our opinion that both FR^{-1} (which effectively measures the level of polarization leakage into $\sigma^{\uparrow\downarrow}$, $\sigma^{\downarrow\uparrow}$) and $T_{^3\mathrm{He}}^{\mathrm{majority}}$ (which indicates the relative count rate observed per time interval) should be given equal weight when deciding on the relative counting times per spin configuration and the preferred time at which to exchange ^{3}He cells. As a very rough guideline, this usually translates into continued usage of a ^{3}He cell with an initial $\wp_{^3\mathrm{He}}(t_0)$ polarization of 0.65 to 0.75 for 2 d if Γ is close to 200 h, and 1 d if Γ is 100 h or less.

10. Concluding remarks

In summary, we have provided a practical experimentally driven algorithm to evaluate and characterize PASANS experiments solely in terms of neutron measurements (summarized in Table 1 as a concise reference), and we have provided the user-friendly program *Pol-Corr* to perform this PASANS polarization-correction procedure. The state of the ^{3}He cell filter can be determined at any time from a series of discrete unpolarized beam transmissions, while polarized transmission measurements additionally allow the polarization efficiency of the supermirror and flipper to be determined. Based on the time stamp associated with each scattering file, the polarization of the correctly associated ^{3}He cell is calculated for the time of data collection, and the scattering files are then combined, fully corrected for polarization and reduced into four ASCII output files, $\sigma^{\uparrow\uparrow}$, $\sigma^{\uparrow\downarrow}$, $\sigma^{\downarrow\downarrow}$ and $\sigma^{\downarrow\uparrow}$, with the aid of *Pol-Corr*. The two-dimensional output format is created such that the files may be viewed on the spot or imported back into the SANS reduction and modeling software (Kline, 2006) for further processing and analysis, such as described by Krycka *et al.* (2012). We feel that this powerful technique for evaluating buried magnetic structures with directional sensitivity is likely to become significantly more popular as the barrier to its usage is lowered.

The authors gratefully acknowledge Yumi Ijiri, Liv Dedon, Cindi Dennis, Andrew Jackson, Sami El Khatib and Mike Fitzsimmons for their vigorous software testing. We also thank Sara Majetich, Ryan Booth, Josep Nogués, Rob Ivkov and Chris Leighton for providing a variety of magnetic systems on which to develop our software, Cosmin Blaga for his aid in setting up the *LabVIEW* framework, and Cedric Gagnon for his efforts in making the PASANS experiments successful. This work utilized facilities supported in part by the US National Science Foundation under agreement No. DMR-0944772. The development of the ^{3}He spin filters was supported in part by the US Department of Energy.

References

Chen, W. C., Erwin, R., McIver, J. W. III, Watson, S., Fu, C. B., Gentile, T. R., Borchers, J. A., Lynn, J. W. & Jones, G. L. (2009). *Physica B*, **404**, 2663–2666.
Gaspar, A. M., Busch, S., Appavou, M.-S., Haeussler, W., Georgii, R., Su, Y. & Doster, W. (2010). *Biochim. Biophys. Acta*, **1804**, 76–82.
Gentile, T. R., Jones, G. L., Thompson, A. K., Barker, J., Glinka, C. J., Hammouda, B. & Lynn, J. W. (2000). *J. Appl. Cryst.* **33**, 771–774.
Honecker, D., Ferdinand, A., Döbrich, F., Dewhurst, C. D., Wiedenmann, A., Gómez-Polo, C., Suzuki, K. & Michels, A. (2010). *Eur. Phys. J. Sect. B*, **76**, 209–213.
Jones, G. L., Dias, F., Collett, B., Chen, W. C., Gentile, T. R., Piccoli, P. M. B., Miller, M. E., Schultz, A. J., Yan, H., Tong, X., Snow, W. M., Lee, W. T., Hoffmann, C. & Thomison, J. (2006). *Physica B*, **385**, 1131–1133.
Keiderling, U. (2002). *Appl. Phys. A*, **74**, S1455–S1457.
Keiderling, U., Wiedenmann, A., Rupp, A., Klenke, J. & Heil, W. (2008). *Meas. Sci. Technol.* **19**, 034009.
Kline, S. R. (2006). *J. Appl. Cryst.* **39**, 895–900.
Krycka, K. L., Booth, R., Borchers, J. A., Chen, W. C., Conlon, C., Gentile, T. R., Hogg, C., Ijiri, Y., Laver, M., Maranville, B. B., Majetich, S. A., Rhyne, J. J. & Watson, S. M. (2009). *Physica B*, **404**, 2561–2564.
Krycka, K. L., Booth, R. A., Hogg, C. R., Ijiri, Y., Borchers, J. A., Chen, W. C., Watson, S. M., Laver, M., Gentile, T. R., Dedon, L. R., Harris, S., Rhyne, J. J. & Majetich, S. A. (2010). *Phys. Rev. Lett.* **104**, 207203.
Krycka, K., Borchers, J., Ijiri, Y., Booth, R. & Majetich, S. (2012). *J. Appl. Cryst.* **45**, 554–565.
Lefebvre, M., Keeler, R. K., Sobie, R. & White, J. (2000). *Nucl. Instrum. Methods Phys. Res. Sect. A*, **451**, 520–528.
Majkrzak, C. (1991). *Handbook of Neutron Scattering*. Berlin: Springer-Verlag.
Michels, A. & Weissmüller, J. (2008). *Rep. Prog. Phys.* **71**, 066501.
Moon, R. M., Riste, T. & Koehler, W. C. (1969). *Phys. Rev.* **181**, 920–931.
Petoukhov, A. K., Andersen, K. H., Jullien, D., Babcock, E., Chastagnier, J., Chung, R., Humblot, H., Lelièvre-Berna, E., Tasset, F., Radu, F., Wolff, M. & Zabel, H. (2006). *Physica B*, **385–386**, 1146–1148.
Schärpf, O. & Capellmann, H. (1993). *Phys. Status Solidi A*, **135**, 359–379.
Schweika, W. (2010). *J. Phys. Conf. Ser.* **211**, 012026.
Wiedenmann, A. (2005). *Physica B*, **356**, 246–253.
Wildes, A. R. (2006). *Neutron News*, **17**(2), 17–25.